Approaching Quantum-Limited Metrology with Imperfect Detectors by Using Weak-Value Amplification

Liang Xu,[1] Zexuan Liu,[1] Animesh Datta,[2] George C. Knee,[2] Jeff S. Lundeen,[3] Yan-qing Lu,[1,*] and Lijian Zhang[1,†]

[1]National Laboratory of Solid State Microstructures, Key Laboratory of Intelligent Optical Sensing and Manipulation, College of Engineering and Applied Sciences, and Collaborative Innovation Center of Advanced Microstructures, Nanjing University, Nanjing 210093, China

[2]Department of Physics, University of Warwick, Coventry CV4 7AL, United Kingdom

[3]Max Planck Centre for Extreme and Quantum Photonics, Department of Physics, University of Ottawa, 25 Templeton Street, Ottawa, Ontario K1N 6N5, Canada

(Received 5 May 2020; accepted 24 July 2020; published 17 August 2020)

Weak-value amplification (WVA) is a metrological protocol that amplifies ultrasmall physical effects. However, the amplified outcomes necessarily occur with highly suppressed probabilities, leading to the extensive debate on whether the overall measurement precision is improved in comparison to that of conventional measurement (CM). Here, we experimentally demonstrate the unambiguous advantages of WVA that overcome practical limitations including noise and saturation of photodetection and maintain a shot-noise-scaling precision for a large range of input light intensity well beyond the dynamic range of the photodetector. The precision achieved by WVA is 6 times higher than that of CM in our setup. Our results clear the way for the widespread use of WVA in applications involving the measurement of small signals including precision metrology and commercial sensors.

DOI: 10.1103/PhysRevLett.125.080501

Introduction.—The precision of optical metrology and sensing is ultimately determined by the quantum fluctuations of light. Quantum-optical states (e.g., N00N states and squeezed states) can improve the precision of parameter estimation from the shot-noise limit (SNL) [1] to the Heisenberg limit (HL) [2,3]. However, such quantum states are very vulnerable to experimental imperfections and are difficult to prepare, especially for large photon numbers [4,5]. Instead, a typical approach to enhance precision is to increase the average photon number $\bar{n}$ of the coherent state. In principle, this scheme can attain a precision at SNL, which scales as $1/\sqrt{\bar{n}}$. In practice, this scaling is a challenge due to the ubiquitous noise of detectors [6]. In particular, the saturation of detectors sets a tight limit on the intensity of the detected light, beyond which the enhancement in the measurement precision by increasing the light intensity is reduced or even eliminated.

Weak-value amplification (WVA), deployed to amplify miniscule physical effects through postselection [7–11], has the potential for enhancing measurement sensitivity and overcoming certain environmental disturbances [12–18]. Yet to date most of works demonstrating the metrological advantages of WVA are attained under theoretical assumptions and experimental conditions different from those of conventional measurement (CM) [19–29]. Identifying the unambiguous advantage of WVA is still under exploration [30]. With ideal setups, WVA can achieve as good precision as CM [31–33]. Crucially, this implies the small number of postselected photons contain almost all of the metrological information. As a result, WVA potentially provides an approach to ensure that the detector operates under the saturation threshold even for a large number of input photons, thereby preserving the shot-noise-scaling precision and outperforming CM [34].

In this work, we demonstrate the capability of the WVA scheme to overcome the precision limit set by the saturation of the detectors. As an example, we experimentally measure a small transverse displacement of an optical beam, which plays an important role in many applications [35,36]. The results confirm that WVA outperforms the CM in terms of precision in the presence of detector noise and saturation. Moreover, the optimal precision of WVA can be attained with a widely tunable probability of postselection, which allows the precision to maintain the shot-noise scaling (i.e., 1.19 times SNL) for a much larger number of input photons, and extends the dynamic range of the measurement system by two orders of magnitude. Our analysis is also applicable to the measurement of other physical parameters [37–39] with different kinds of photodetectors.

Theoretical framework.—Figure 1 describes the measurement of the displacement g with a standard Gaussian meter state (MS) $|\Phi_0\rangle = \int dq 1/(2\pi\sigma^2)^{1/4} \exp[-q^2/(4\sigma^2)]|q\rangle = \int dp (2\sigma^2/\pi)^{1/4} \exp(-\sigma^2 p^2)|p\rangle$, where $|q\rangle$ and $|p\rangle$ are the eigenstates of the position operator $\hat{Q}$ and the momentum operator $\hat{P}$, respectively. In CM, this meter state is evolved

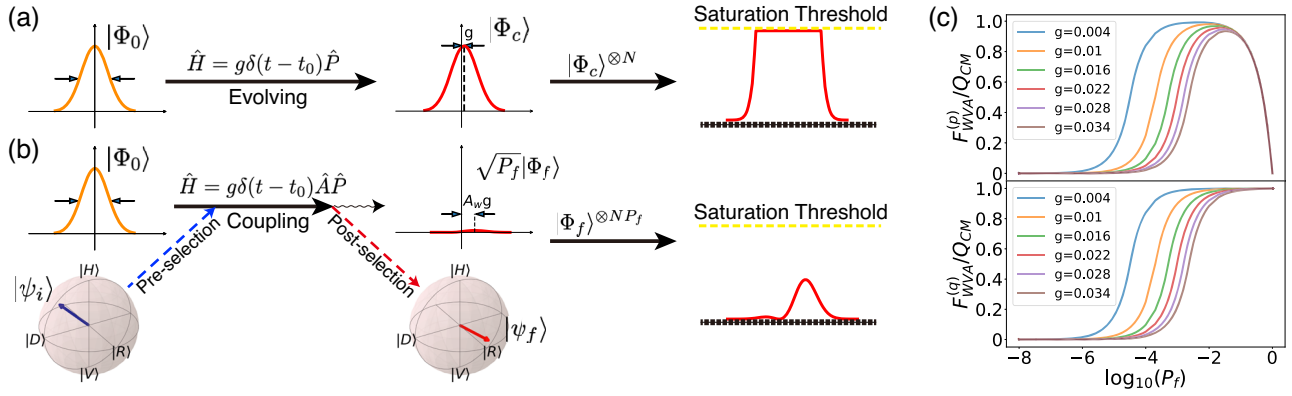

FIG. 1. Comparison between the conventional measurement and the weak-value amplification. (a) Schematic for the conventional measurement and (b) weak-value amplification of parameter g with a Gaussian meter state in the position degree of freedom of photons. With a large number of input photons, detector saturation causes distortion in the measurement outcome in CM, while WVA avoids the saturation due to the reduced photon number with postselection. The upper (lower) figure in (c) plots the ratio of the maximal classical Fisher information $F^{(p)}_{\mathrm{WVA}}$ ($F^{(q)}_{\mathrm{WVA}}$) in WVA with completely imaginary (real) weak value to the quantum Fisher information Q_{CM} of CM with ideal detection as a function of the successful postselection probability P_f for different values of g. The width of the Gaussian meter state is $2\sigma = 1$.

under the Hamiltonian $\hat{H} = g\delta(t-t_0)\hat{P}$, which leads to the final state $|\Phi_c\rangle = \int dq 1/(2\pi\sigma^2)^{1/4}\exp[-(q-g)^2/(4\sigma^2)]|q\rangle$ with a displacement g in q. In contrast, WVA is regarded as an ancilla-assisted metrological scheme. A two-level quantum system (QS) with preselected state $|\psi_i\rangle = \cos(\theta_i/2)|0\rangle + \sin(\theta_i/2)e^{i\phi_i}|1\rangle$ is coupled to the meter state by the Hamiltonian $\hat{H} = g\delta(t-t_0)\hat{A}\,\hat{P}$ and then projected onto the post-selected state $|\psi_f\rangle = \cos(\theta_f/2)|0\rangle + \sin(\theta_f/2)e^{i\phi_f}|1\rangle$, resulting in the final MS $|\Phi_f\rangle$ with the success probability P_f, where $\hat{A}$ is an observable of QS. In the weak interaction regime ($g \ll \sigma$), the average shift of $|\Phi_f\rangle$ in q or p space are, respectively, approximated as $g\mathrm{Re}(A_w)$ and $g\mathrm{Im}(A_w)/(2\sigma^2)$, where A_w is the "weak value" of the observable $\hat{A}$, given by $A_w = \langle\psi_f|\hat{A}|\psi_i\rangle/\langle\psi_f|\psi_i\rangle$. When the denominator $\langle\psi_f|\psi_i\rangle$ becomes small, A_w can become large giving rise to the amplification effect.

To acquire the information about g, we perform measurement on the final states $|\Phi_c\rangle$ of CM and $|\Phi_f\rangle$ of WVA. According to the Cramér-Rao bound (CRB), the best precision of estimating g from ν times of repetitive measurement is given by $\delta^2 g \geq 1/(\nu F)$, where $\delta^2 g$ is the variance of the estimator of g and F is the Fisher information (FI) [40]. The maximum FI, known as the quantum Fisher information (QFI), can be achieved with the optimal measurement on the state. For CM, a measurement in the position q on the $|\Phi_c\rangle$ is optimal such that the FI F_{CM} of the measured distributions equal the QFI $Q_{\mathrm{CM}} = 1/\sigma^2$. The QFI of WVA Q_{WVA} depends on the $|\psi_i\rangle$ and $|\psi_f\rangle$ but the maximal $Q_{\mathrm{WVA}} = Q_{\mathrm{CM}}$. In addition, the measurement on $|\Phi_f\rangle$ in the q (p) space proves to be optimal if the weak value is completely real (imaginary) such that the FI $F^{(q)}_{\mathrm{WVA}} = Q_{\mathrm{WVA}}$ ($F^{(p)}_{\mathrm{WVA}} = Q_{\mathrm{WVA}}$) [41]. Therefore, both CM and WVA are optimized, leading to $F_{\mathrm{CM}} = F_{\mathrm{WVA}}$. However, a large number of input photons is more likely to saturate the detectors in CM than in WVA, as illustrated in Fig. 1, which causes distortion of the measurement on $|\Phi_c\rangle$ and diminishes F_{CM}. This provides a potential advantage of WVA over CM.

We denote the WVA with completely real and completely imaginary weak values as RWVA and IWVA, respectively. Here, our aim is to acquire as high a precision as possible while detecting a limited number of photons. We maximize the FI $F^{(q)}_{\mathrm{WVA}}$ ($F^{(p)}_{\mathrm{WVA}}$) normalized to Q_{CM} over a range of P_f for different g [41], which is shown in Fig. 1(c). The RWVA shows obvious advantages in that the increase of P_f always promises an enhanced precision. For example, with parameters $g = 0.01$ and $\sigma = 0.5$ in the RWVA scheme, $F^{(q)}_{\mathrm{WVA}}$ can attain over 99% of Q_{CM} over a large range (1% to 100%) of the input photons being detected. This incredible property provides us with great flexibility for the choice of P_f. Consequently, WVA can operate in an intensity range well above the noise floor but under the saturation level of detectors, and simultaneously, maintain the metrological information. By contrast, there is a peak value of $F^{(p)}_{\mathrm{WVA}}/Q_{\mathrm{CM}}$ with the change of P_f in IWVA. Indeed, Ref. [44] also shows that in IWVA, the optimal choice of P_f (and, hence, the pre- and postselected states) is sensitive to the parameter g. It follows that one must have some prior knowledge of g in order to design a measurement system using IWVA. Consequently, we choose to implement the optimal RWVA scheme and make a comparison to CM in our experiment.

Experiment.—The experimental setup is shown in Fig. 2. The polarization and spatial degrees of freedom of the CW laser beam at 633 nm with the TEM00 mode (beam width $\sigma = 0.472$ mm) are used as the ancillary QS ($|0\rangle \to |H\rangle, |1\rangle \to |V\rangle$) and the Gaussian MS, respectively.

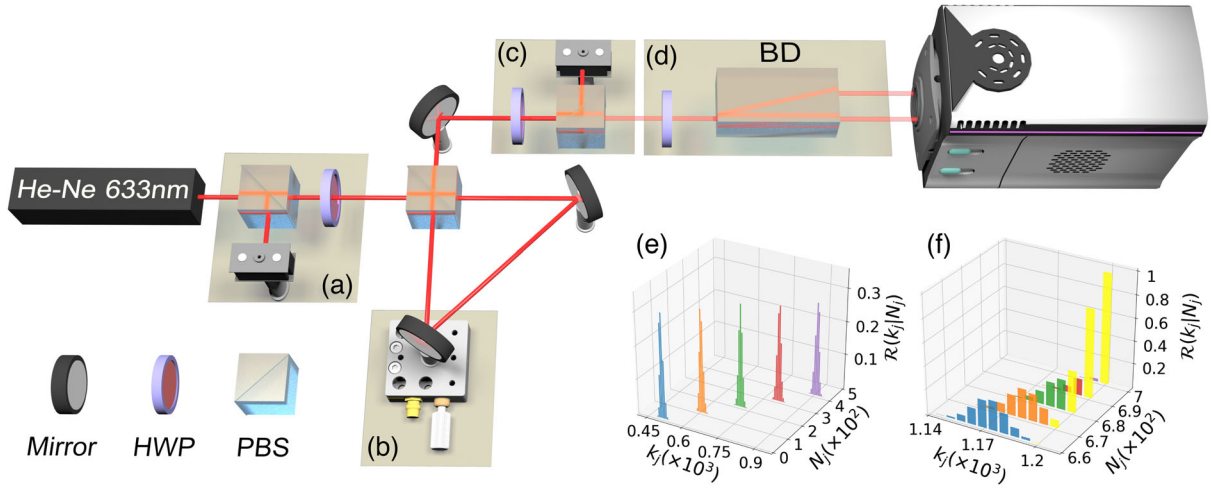

FIG. 2. Experimental setup and detector calibration. Module (a) and (c) perform the pre- and postselection of the polarization of photons. The displacement of the mirror in module (b) couples the polarization and the spatial degree of freedom. A HWP and a polarizing beam displacer (BD) in module (d) create two copies of the output beam in order to cancel out the adverse effects of beam jitter and turbulence. Plots (e) and (f) give examples of the measured response matrix of the CCD, i.e., the probability distribution $\mathcal{R}(k_j|N_j)$ of pixel readout k_j when N_j photoelectrons are generated, far from and close to saturation, respectively.

The input photons pass through a polarizing beam splitter (PBS) and a half-wave plate (HWP) to prepare the preselected state. The photons in the $|H\rangle$ ($|V\rangle$) state go clockwise (anticlockwise) in the Sagnac interferometer. A slight displacement of the mirror results in the coupling between the QS and the meter state. After recombination at the output port, a HWP and a PBS performs the postselection. The meter state is then measured in the position q space by a scientific CCD (Andor, iStar CCD 05577H) with pixel size 13 μm $\times$ 13 μm. If the total average number of photons in the Gaussian beam is $\bar{n}_t$ per exposure, the jth pixel of the CCD is expected to receive $\bar{n}_j^{\mathrm{WVA}}(g) = P_f \bar{n}_t \int_j dq |\langle q|\Phi_f\rangle|^2$ and $\bar{n}_j^{\mathrm{CM}}(g) = \bar{n}_t \int_j dq |\langle q|\Phi_c\rangle|^2$ photons in the WVA and CM schemes, respectively. Since the beam is in a coherent state, the exact number N_j of the registered photons (i.e., photoelectrons) at the jth pixel follows a Poisson distribution $P(N_j|\eta\bar{n}_j, g)$, where $\eta = 0.125$ is the detection efficiency of the CCD. Additionally, due to various kinds of electrical noise, the response of CCD can be described by a conditional probability distribution $\mathcal{R}(k_j|N_j)$, where k_j is the readout at the jth pixel. The readout k_j contains the contributions from the dark noise K_d, N_j, and the extra classical noise K_a. The calibration shows that K_d and K_a follow normal distributions $K_d \sim \mathcal{N}(\mu_d, \sigma_d^2)$ and $K_a \sim \mathcal{N}(0, \sigma_a^2)$, in which σ_a grows with $\bar{n}_j$, following $\ln(\sigma_a^2) = a\ln(\bar{n}_j) + b$ with $a = 1.19$ and $b = -4.39$. Thus, $\mathcal{R}(k_j|N_j)$ is obtained by the convolution of dark noise and the extra classical noise distributions. Given the saturation threshold k_s, the response at the threshold is transformed to $\mathcal{R}(k_s|N_j) = \sum_{k_j \geq k_s} \mathcal{R}(k_j|N_j)$. We present certain $\mathcal{R}(k_j|N_j)$ of our detectors in Figs. 2(e) and 2(f). The response model of CCD here is similar to that in Ref. [34] with digitization and pixel noise.

Taking all of the mentioned factors into consideration, the conditional probability distribution of k_j that depends on g is given by

$$P(k_j|g) = \sum_{N_j} \mathcal{R}(k_j|N_j) P(N_j|\eta\bar{n}_j, g). \tag{1}$$

Subsequently, the classical Fisher information for g of the whole CCD array can be calculated from $P(k_j|g)$ and simplified as

$$F(g) = \sum_j \frac{\eta}{\bar{n}_j} \left(\frac{d\bar{n}_j}{dg}\right)^2 \Gamma(\mathcal{R}, \bar{n}_j), \tag{2}$$

in which the coefficient $\Gamma(\mathcal{R}, \bar{n}_j)$ can be treated as the signal-to-noise ratio at the jth pixel, taking into account the fundamental quantum fluctuations of light and probabilistic response of the CCD. When the $\bar{n}_j$ in Eq. (2) is replaced by $\bar{n}_j^{\mathrm{CM}}$ or $\bar{n}_j^{\mathrm{WVA}}$, we can obtain the FI of CM or WVA, respectively. Equation (2) also implies that the response of the CCD $\mathcal{R}(k_j|N_j)$ plays a vital role in acquiring the Fisher information $F(g)$. For example, when the pixel approaches saturation, $\Gamma(\mathcal{R}, \bar{n}_j)$ tends to zero, leading to a considerable reduction in FI [41].

To estimate the parameter g, we apply the maximum likelihood estimation (MLE) with the likelihood function

$$\mathcal{L}(g) = \prod_{l=1}^{\nu} \prod_{j=1}^{\tau} \left[\sum_{N_{lj}} \mathcal{R}_s(k_{lj}|N_{lj}) P(N_{lj}|\eta\bar{n}_{lj}, g)\right], \tag{3}$$

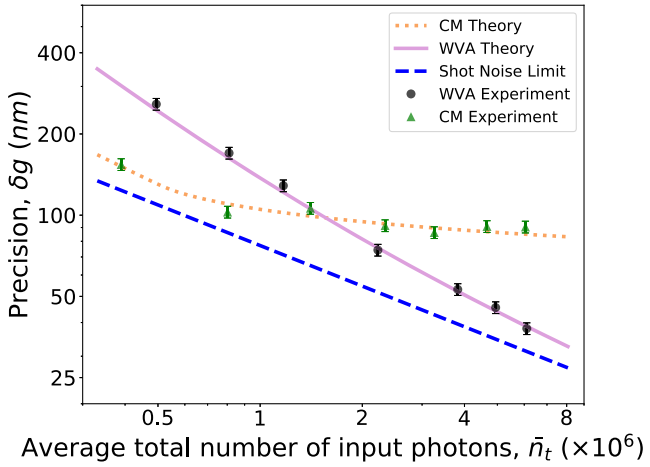

FIG. 3. Comparison between the precision of conventional measurement and that of weak-value amplification using maximum likelihood estimation. The theoretical results of MLE are determined by the Cramér-Rao bound. All error bars refer to ±1 s.d. and are calculated from the fourth moment of the estimated parameter g. The "shot noise limit" is determined by $\delta g = \sigma/\sqrt{\nu\eta\bar{n}_t}$. The other two estimation methods, split-detection (SD) and center-of-mass, follow a similar trend but offer reduced precision compared to MLE [41].

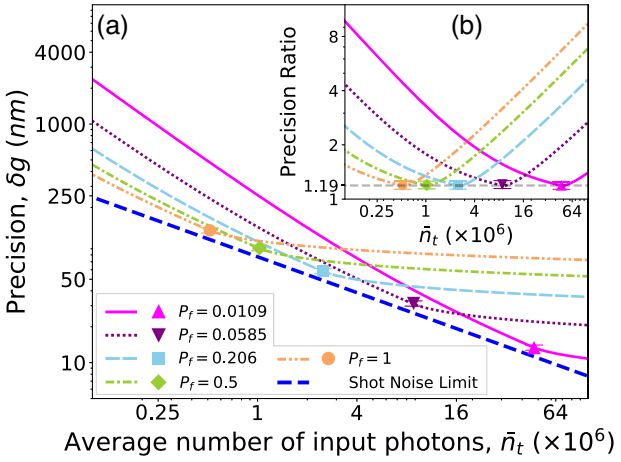

FIG. 4. Weak-value amplification with different success probabilities of postselection P_f. (a) The precision of WVA with different P_f and average total number of input photons $\bar{n}_t$. The error bars refer to ±1 s.d. In (b) we plot the ratio of the precision in WVA to the shot-noise limit. In our experiment, we implement the optimal precision WVA scheme which has the minimum ratio 1.19 for each specified $\bar{n}_t$. The theoretical results (lines) are determined by the Cramér-Rao bound and the experimental results (points) are obtained using maximum likelihood estimation.

where $\nu = 300$ and $\tau = 330$ are the total number of frames and pixels in one estimate, respectively. The exposure time of each frame is 1 ms. To obtain the precision of the estimation δg, we employ a bootstrap method [42,43,45] with the following three steps: (i) ν frames are independently and uniformly sampled from a set of 6000 frames to obtain one estimate of g. (ii) Repeat (i) for $B = 200$ times to get estimates $\{g_i\}$ with $i = 1 \ldots B$. (iii) Calculate the standard deviation δg of $\{g_i\}$ as an estimation of the measurement precision. Since MLE is known to be able to saturate the Cramér-Rao bound asymptotically, the theoretical precision of WVA is given by $\delta g_{\mathrm{MLE}} = 1/\sqrt{\nu F(g)}$.

We first compare the precision of CM and WVA with the identical MS for a range of the average total number of input photons $\bar{n}_t$. In WVA, we set $\theta_i = -\theta_f = 76°$, $P_f = 0.0585$, and $A_w = 4.13$. As Fig. 3 shows, CM outperforms WVA when $\bar{n}_t$ is small because CM collects all the input photons, which helps diminish the impact of dark noise. However, as $\bar{n}_t$ gets large, saturation begins to occur in the CM scheme, thereby restricting further improvements of precision. In contrast, by concentrating the metrological information into many fewer photons, WVA avoids saturation and maintains the increase of precision for a large $\bar{n}_t$. We also give an intuitive illustration in which the FIs distributed in each pixel of CCD with the increase of total input photons are compared between CM and WVA [41]. As a comparison, two other methods, split-detection (SD) estimation, and center-of-mass estimation, are applied to estimate g and the results are given in Ref. [41]. Both of them show a trend similar to that of MLE but with reduced precision, which conforms to our intuition that a more accurate model taking into account more characteristics of the experimental apparatus tends to extract more information from a particular probability distribution.

Furthermore, we have also compared the precision of WVA with $P_f = 0.0109, 0.0585, 0.206, 0.5, 1$ by setting $\theta_i = -\theta_f = 84°, 76°, 63°, 45°, 0°$ and $\phi_i = \phi_f = 0$, respectively. The MLE results are shown in Fig. 4. We find that for a specified average number of input photons $\bar{n}_t$, there exists the optimal choice of P_f to achieve the best precision due to the trade-off between resisting the various types of noise and avoiding saturation in photodetectors. In our experiment, we adapt the P_f and obtain the optimal precision for each $\bar{n}_t$ with MLE, which is 1.19 times the SNL since detector noise and imperfections cannot be completely avoided [41]. Besides, SD and center-of-mass estimators give the optimal precision 1.29 and 1.67 times SNL.

Discussion.—Although keeping a small postselection probability P_f avoids the detector saturation to a large extent, this may not always be the optimal strategy in the presence of detector noise. The true power of WVA is to adjust P_f over a large range while maintaining the metrological information, which allows us to minimize the overall detector imperfections and maximize the precision. This is also the reason for the advantage of RWVA over IWVA since the former provides a greater flexibility for the choice of P_f.

Compared to previous works that focus on the study of the amplification effect and signal-to-noise ratio of

WVA [12,14,15], our work investigates WVA from the parameter-estimation perspective using the FI as the metric, which is directly related to the measurement precision. We optimize the configurations that maximize the FI for both WVA and CM to provide a fair comparison and verify the unambiguous benefit of WVA. The careful calibration of all the detector noise and imperfections allows us to apply MLE, which saturates Cramér-Rao bound. Our results provide compelling evidence for the metrological advantages of WVA over CM in the presence of detector noise and saturation.

In summary, by preserving all the metrological information with a tunable fraction of postselected photons, weak-value amplification (WVA) promises to be a key technique for extending the dynamic range of a measurement system. More generally, we have shown that it is possible to channel metrological information into particular aspects of a sensor output signal, thereby allowing one to match them to the detector aspects that have the best specifications (e.g., resolution, noise in a certain intensity range, bit depth, etc.). For now, we have opened a path to its application in a wide variety of commercial, industrial, and scientific sensors and instruments.

The authors thank B. J. Smith and L. L Sánchez-Soto for assistance and fruitful discussions. This work was supported by the National Key Research and Development Program of China (Grants No. 2017YFA0303703 and No. 2018YFA0306202) and the National Natural Science Foundation of China (Grants No. 91836303, No. 61975077, No. 61490711, and No. 11690032) and Fundamental Research Funds for the Central Universities (Grant No. 020214380068). A. D. is supported by the UK EPSRC (EP/K04057X/2), the UK National Quantum Technologies Programme (EP/M01326X/1, EP/M013243/1) and the University of Warwick Global Partnership Fund.

*yqlu@nju.edu.cn
†lijian.zhang@nju.edu.cn

[1] S. L. Braunstein, Phys. Rev. Lett. **69**, 3598 (1992).
[2] P. Walther, J.-W. Pan, M. Aspelmeyer, R. Ursin, S. Gasparoni, and A. Zeilinger, Nature (London) **429**, 158 (2004).
[3] M. Xiao, L.-A. Wu, and H. J. Kimble, Phys. Rev. Lett. **59**, 278 (1987).
[4] V. Giovannetti, S. Lloyd, and L. Maccone, Nat. Photonics **5**, 222 (2011).
[5] R. Demkowicz-Dobrzański, J. Kołodyński, and M. Guţă, Nat. Commun. **3**, 1063 (2012).
[6] J. R. Janesick *et al.*, *Scientific Charge-Coupled Devices* (SPIE Press, Bellingham, 2001).
[7] O. Hosten and P. Kwiat, Science **319**, 787 (2008).
[8] P. B. Dixon, D. J. Starling, A. N. Jordan, and J. C. Howell, Phys. Rev. Lett. **102**, 173601 (2009).
[9] G. Strübi and C. Bruder, Phys. Rev. Lett. **110**, 083605 (2013).
[10] O. S. Magaña-Loaiza, M. Mirhosseini, B. Rodenburg, and R. W. Boyd, Phys. Rev. Lett. **112**, 200401 (2014).
[11] X.-Y. Xu, Y. Kedem, K. Sun, L. Vaidman, C.-F. Li, and G.-C. Guo, Phys. Rev. Lett. **111**, 033604 (2013).
[12] S. Pang and T. A. Brun, Phys. Rev. Lett. **115**, 120401 (2015).
[13] S. Pang, J. R. G. Alonso, T. A. Brun, and A. N. Jordan, Phys. Rev. A **94**, 012329 (2016).
[14] Y. Kedem, Phys. Rev. A **85**, 060102(R) (2012).
[15] D. J. Starling, P. B. Dixon, A. N. Jordan, and J. C. Howell, Phys. Rev. A **80**, 041803(R) (2009).
[16] S. Pang and T. A. Brun, Phys. Rev. A **92**, 012120 (2015).
[17] A. Nishizawa, K. Nakamura, and M.-K. Fujimoto, Phys. Rev. A **85**, 062108 (2012).
[18] A. N. Jordan, J. Martínez-Rincón, and J. C. Howell, Phys. Rev. X **4**, 011031 (2014).
[19] J. P. Torres and L. J. Salazar-Serrano, Sci. Rep. **6**, 19702 (2016).
[20] J. Combes, C. Ferrie, Z. Jiang, and C. M. Caves, Phys. Rev. A **89**, 052117 (2014).
[21] L. Vaidman, Phil. Trans. R. Soc. A **375**, 20160395 (2017).
[22] J. Lee and I. Tsutsui, Quantum Stud. Math. Found. **1**, 65 (2014).
[23] C. Ferrie and J. Combes, Phys. Rev. Lett. **112**, 040406 (2014).
[24] G. I. Viza, J. Martínez-Rincón, G. B. Alves, A. N. Jordan, and J. C. Howell, Phys. Rev. A **92**, 032127 (2015).
[25] N. Brunner and C. Simon, Phys. Rev. Lett. **105**, 010405 (2010).
[26] G. C. Knee and E. M. Gauger, Phys. Rev. X **4**, 011032 (2014).
[27] J. Dressel, M. Malik, F. M. Miatto, A. N. Jordan, and R. W. Boyd, Rev. Mod. Phys. **86**, 307 (2014).
[28] G. C. Knee, J. Combes, C. Ferrie, and E. M. Gauger, Quantum Meas. Quantum Metrol. **3**, 011031 (2014).
[29] G. C. Knee and G. A. D. Briggs, Quantum Stud. Math. Found. **5**, 505 (2018).
[30] D. R. M. Arvidsson-Shukur, N. Y. Halpern, H. V. Lepage, A. A. Lasek, C. H. W. Barnes, and S. Lloyd, arXiv: 1903.02563.
[31] L. Zhang, A. Datta, and I. A. Walmsley, Phys. Rev. Lett. **114**, 210801 (2015).
[32] S. Tanaka and N. Yamamoto, Phys. Rev. A **88**, 042116 (2013).
[33] G. B. Alves, B. M. Escher, R. L. de Matos Filho, N. Zagury, and L. Davidovich, Phys. Rev. A **91**, 062107 (2015).
[34] J. Harris, R. W. Boyd, and J. S. Lundeen, Phys. Rev. Lett. **118**, 070802 (2017).
[35] D. Rugar and P. Hansma, Phys. Today **43**, No. 10, 23 (1990).
[36] S. B. Howell, *Handbook of CCD Astronomy* (Cambridge University Press, Cambridge, 2006).
[37] G. Strübi and C. Bruder, Phys. Rev. Lett. **110**, 083605 (2013).
[38] O. S. Magaña-Loaiza, M. Mirhosseini, B. Rodenburg, and R. W. Boyd, Phys. Rev. Lett. **112**, 200401 (2014).
[39] X.-Y. Xu, Y. Kedem, K. Sun, L. Vaidman, C.-F. Li, and G.-C. Guo, Phys. Rev. Lett. **111**, 033604 (2013).
[40] H. Cramer, *Mathematical Methods of Statistics* (Princeton University Press, Princeton, 1946).

[41] See Supplemental Material at http://link.aps.org/supplemental/10.1103/PhysRevLett.125.080501 for the theoretical derivations and experimental details, which includes Refs. [42,43].
[42] R. W. Johnson, Teach. Stat. **23**, 49 (2001).
[43] S. L. Braunstein, J. Phys. A **25**, 3813 (1992).
[44] F. Li, J. Huang, and G. Zeng, Phys. Rev. A **96**, 032112 (2017).
[45] A. C. Davison and D. V. Hinkley, *Bootstrap Methods and their Application* (Cambridge University Press, Cambridge, 1997).